



Excited state properties of two unusual thermally activated delayed fluorescence molecules: A theoretical investigation

Jiancai Leng^a, Zhiyuan Zhang^a, Yujin Zhang^a, Jie Sun^{a,*}, Hong Ma^{b,*}

^a School of Science, Qilu University of Technology (Shandong Academy of Sciences), Jinan 250353, China

^b Shandong Provincial Key Laboratory of Optics and Photonic Device, College of Physics and Electronics, Shandong Normal University, Jinan 250014, China

ARTICLE INFO

Keywords:

Thermally activated delayed fluorescence
Singlet-triplet energy gap
Intersystem crossing and reverse intersystem crossing
Huang-Rhys factor

ABSTRACT

High efficient thermally activated delayed fluorescence (TADF) emitters containing 2,4-bis(3-(9H-carbazol-9-yl)-9H-carbazol-9-yl)-6-phenyl-1,3,5-triazine (CC2TA) and 2-biphenyl-4,6-bis(12-phenylindolo[2,3-*a*] carbazole-11-yl)-1,3,5-triazine (PIC-TRZ) exhibit an internal quantum efficiency (η_{int}) of 56% and 34% respectively, which breaks the traditional limitation of 25%. CC2TA and PIC-TRZ are two special cases in Adachi's work and they are not in accordance with their proposed regulations. Based on the newly-proposed optimal Hartree-Fock percentage (OHF) method, we investigate the adiabatic energy gap (ΔE_{st}) between the first singlet (S_1) and triplet (T_1) excited state as well as the absorption and emission spectra for CC2TA and PIC-TRZ. Moreover, we investigate the intersystem crossing (ISC) and reverse intersystem crossing (RISC) processes to illustrate the internal transfer mechanism of singlet and triplet excitons. Results show that our calculated data are consistent with the experimental values. RMSD and Huang-Rhys factor are smaller for PIC-TRZ than these for CC2TA, this results the non-radiative decay rate from S_1 to ground state (S_0) is decreased for PIC-TRZ. Moreover, the ISC and RISC processes are multi-step processes with the incorporation of intermediate energy level between S_1 and T_1 . Our work could provide a clear guidance for molecular luminescence simulations and the design of high efficient TADF molecules.

1. Introduction

Recently, thermally activated delayed fluorescence (TADF) emitters have attracted much attention not only because of their low-cost manufacture without using rare metals and potential for high electroluminescence (EL) efficiency but also they can effectively convert triplet excitons into singlet excitons which is named as delayed fluorescence [1–5]. TADF materials have broken the limitation of the internal quantum efficiency for traditional fluorescence OLEDs whose maximum utilization of singlet excitons is 25% due to the branching ratio of the singlet and triplet excitons (1:3), so TADF materials are considered as the next generation of lighting and display devices [6,7]. For effective TADF molecules, a small energy gap (ΔE_{st}) between the lowest singlet excited state (S_1) and lowest triplet excited state (T_1) is important to achieve high reverse intersystem crossing (RISC) process, because the RISC rate can be represented by $K_{\text{RISC}} \approx 1/3 \exp(-\Delta E_{\text{st}}/K_{\text{B}}T)$ where K_{B} denotes the Boltzmann constant and T is temperature. Thus, harvesting the non-radiative triplet excitons generated by carrier recombination at room temperature is an important issue for developing high efficient thermally activated delayed fluorescence organic light emitting diodes

(TADF-OLEDs), and it is necessary to investigate the photophysical properties of TADF molecules.

Herein, we choose two experimental synthesized molecules of 2,4-bis(3-(9H-carbazol-9-yl)-9H-carbazol-9-yl)-6-phenyl-1,3,5-triazine (CC2TA) and 2-biphenyl-4,6-bis(12-phenylindolo[2,3-*a*] carbazole-11-yl)-1,3,5-triazine (PIC-TRZ) as representative molecules due to their similar structures and unique properties in previous research [8,9]. Based on the optimized structures, we identify the optimal functional for two molecules respectively. Furthermore, we calculate the radiative rate, non-radiative rate from lowest singlet excited state (S_1) to ground state (S_0) and the intersystem crossing (ISC) rate, reverse intersystem crossing (RISC) rate between lowest singlet excited state and triplet excited state (T_1) as well as the phosphorescence rate. Through our calculation, we analyze the excited states properties and demonstrate that the additional channel between S_1 and T_1 can promote the ISC and RISC processes for CC2TA and PIC-TRZ. This could provide a clear guidance for molecular luminescence simulations and the design of high efficient TADF molecules.

* Corresponding authors.

E-mail addresses: 676528842@qq.com (J. Sun), mahong@sdu.edu.cn (H. Ma).

<https://doi.org/10.1016/j.jlumin.2018.07.012>

Received 24 January 2018; Received in revised form 23 June 2018; Accepted 5 July 2018

Available online 06 July 2018

0022-2313/ © 2018 Published by Elsevier B.V.

2. Theoretical method

The photoluminescence quantum efficiencies of prompt fluorescence (PF) efficiency (Φ_{PF}) can be written as $\Phi_{PF} = \frac{k_r}{k_r + k_{nr} + k_{ISC}}$, and k_r is the radiative decay rate from S_1 to ground state (S_0), k_{nr} is the non-radiative decay rate from S_1 to S_0 and k_{ISC} is the ISC rate from S_1 to T_1 . As for the thermally activated delayed fluorescence (TADF) efficiency (Φ_{TADF}), it is written as $\Phi_{TADF} = \frac{\Phi_{ISC}\Phi_{RISC}}{1 - \Phi_{ISC}\Phi_{RISC}}\Phi_{PF}$, where Φ_{ISC} and Φ_{RISC} are ISC efficiency and RISC efficiency respectively. Thus, in order to obtain the luminescence efficiency, we should first calculate the rate parameters [10].

For the radiative decay rate k_r , it is calculated by Einstein spontaneous emission rate equation, which is written as

$$k_r = \frac{f \Delta E_{fi}^2}{1.499} \quad (1)$$

where the f is oscillator strength without unit dimension and ΔE_{fi} is written as the form of wave number (cm^{-1}).

According to the first-order perturbation theory and the Fermi's golden rule (FGR), the non-radiative decay rate can be written as

$$k_{nr} = \frac{2\pi}{\hbar^2} \sum_{i,v} P_{iv} |H_{fi,iv}|^2 \delta(E_{iv} - E_{fi}). \quad (2)$$

Here P_{iv} is the initial state Boltzmann distribution function and H is the interaction between two different Born-Oppenheimer states, it contains two components

$$\hat{H}\Psi_{iv} = \hat{H}^{BO}\Phi_i(r, Q)\Theta_{iv}(Q) + \hat{H}^{SO}\Phi_i(r, Q)\Theta_{iv}(Q). \quad (3)$$

where \hat{H}^{BO} represents the nonadiabatic coupling and \hat{H}^{SO} denotes the spin-orbit coupling.

Based on the Franck-Condon principle and applying the Fourier transform of the delta function, the non-radiative decay rate constant from S_1 to S_0 can be written as

$$k_{nr} = \sum_{kl} \frac{1}{\hbar^2} R_{kl} \int_{-\infty}^{\infty} dt [e^{i\omega_{if}t} Z_i^{-1} \rho_{IC}(t, T)]. \quad (4)$$

Here $\rho_{IC}(t, T)$ is the thermal vibration correlation function (TVCF). Similarly, the intersystem crossing rate constant between two electronic states with different spin states is written as

$$k_{ISC} = \frac{1}{\hbar^2} \langle \Phi_f \hat{H}^{SO} \Phi_i \rangle \int_{-\infty}^{\infty} dt [e^{i\omega_{if}t} Z_i^{-1} \rho_{ISC}(t, T)]. \quad (5)$$

Both the methodology and application of this formalism can be found in Peng's and Shuai's works [11–15].

3. Computational details

Theoretical study and quantitative analysis to the decay processes of the electronic excited states have important directive significance to design high performance molecules. To investigate the electronic states of CC2TA and PIC-TRZ whose basic structures are shown in Fig. 1, the optimal Hartree-Fock (OHF) method, which has been proved reliable for the calculations of the excitation properties, is adopted [16]. In this method, the transfer charge q is first calculated based on the optimized ground state with Multiwfn (a multifunctional wavefunction analyzer) [17]. Then, the optimal functional is determined according to the relation of HF% = 42*q, where HF% represents the component of the HF in the functionals. So, the functional of PBE38 and PBE33 are selected for CC2TA and PIC-TRZ respectively. The relationship was first proposed by Adachi's group, which was obtained based on the study of 17 molecules [16]. For more details, one can refer to the initial article. Thus, the geometry optimizations and frequency calculations are carried out for S_0 and T_1 through density functional theory (DFT), while for S_1 , time-dependent density functional theory (TD-DFT) is applied. All these calculations are performed by GAUSSIAN09 program with the

optimal functional and 6-31G(d) basis set in toluene [18]. Besides, the spin-orbit coupling constant is obtained by Dalton 2013 software [19]. Finally, the non-radiative rates of polyatomic molecules from S_1 to S_0 and non-radiative rates from T_1 to S_0 are carried out by MOMAP (Molecular Materials Property Prediction Package) promoted by the Institute of Chemistry Chinese Academy of Sciences and Department of Chemistry in Tsinghua University [20–22].

4. Results and discussions

4.1. Vertical excitation energy and adiabatic excitation energy

In this article, we calculate the vertical excitation energy and the adiabatic excitation energy for different situations, so we need to know their different physical processes exactly which are displayed in Fig. 2. Note that we neglect differences in zero point vibrational energies (ZPVE) between the ground and excited states, because ZPVE are small and rather independent of the basis sets and the functional issues. Vertical excitation energies from S_0 to S_1 and T_1 of the molecules are defined as $E_{VA}(S_1) = E(S_1)/E(S_0) - E(S_0)$ and $E_{VA}(T_1) = E(T_1)/E(S_0) - E(S_0)$, where ' $E(X)/E(S_0)$ ' is the excitation energy calculated at the optimized geometry of the ground state S_0 . The vertical singlet-triplet splitting is logically written as $\Delta E_{ST} = E_{VA}(S_1) - E_{VA}(T_1)$ which is corresponding well with the A-B-C transition process shown in Fig. 2. In Adachi's initial article, the energy gap between S_1 and T_1 for CC2TA (60 meV) is calculated by the abovementioned method. Actually, this is a vertical energy gap.

As for the adiabatic excitation energy, it is calculated by the following expressions: $E_{00}(S_1) = E(S_1) - E(S_0)$ and $E_{00}(T_1) = E(T_1) - E(S_0)$, where the $E(S_1)$ and $E(T_1)$ is the minimum energy value at the excitation potential energy surface which is marked as D and E in Fig. 2. So the energy gap between S_1 and T_1 is expressed as the energy difference between D and E . According to the abovementioned equation, if we want to calculate the adiabatic energy gap between S_1 and T_1 , we should know the accurate energy of involved excited states. Thus, the optimization of excited state is needed.

Based on the abovementioned difference between vertical excitation energy and adiabatic excitation energy, we use the optimal functional to calculate the excitation energy of S_1 and T_1 for CC2TA and PIC-TRZ. Here, CC2TA and PIC-TRZ are two special cases in Adachi's work, because their calculated energy gaps by OHF method are not consistent with the experimental results and do not in accordance with their proposed regulations. In this work, we obtain the adiabatic energy between S_1 and T_1 through optimizing the excited state by selected functional rather than the initial approach method proposed by Adachi's group. All results are collected in Table 1. Results show that the calculated ΔE_{ST} is 0.21 eV and 0.20 eV for CC2TA and PIC-TRZ respectively, and they are all corresponding well with their experimental values. Moreover, the calculated adiabatic excitation energies of $E_{00}(S_1)$ and $E_{00}(T_1)$ are also consistent with the experimental data. This indicates the advantage of our method in investigating photophysical properties of CC2TA and PIC-TRZ.

4.2. Frontier molecular orbitals and absorption-emission spectrum

To understand the electron and geometrical structures of CC2TA and PIC-TRZ, quantum chemical calculations are performed. Based on optimized structure, the highest occupied molecular orbital (HOMO) and the lowest unoccupied molecular orbital (LUMO) are drawn in Fig. 3. For CC2TA, HOMO is mainly distributed over the outermost carbazolyl units, whereas LUMO is localized on the central electron-accepting triazine and its phenyl substituent. As for PIC-TRZ, HOMO is mainly distributed on indolocarbazole donor unit and LUMO is localized on biphenyl triazole acceptor unit. Thus, small overlap between HOMO and LUMO can be seen for two molecules. According to the equation $K_{RISC} \propto \exp(-\Delta E_{ST}/(K_B T))$, the reverse intersystem crossing rate

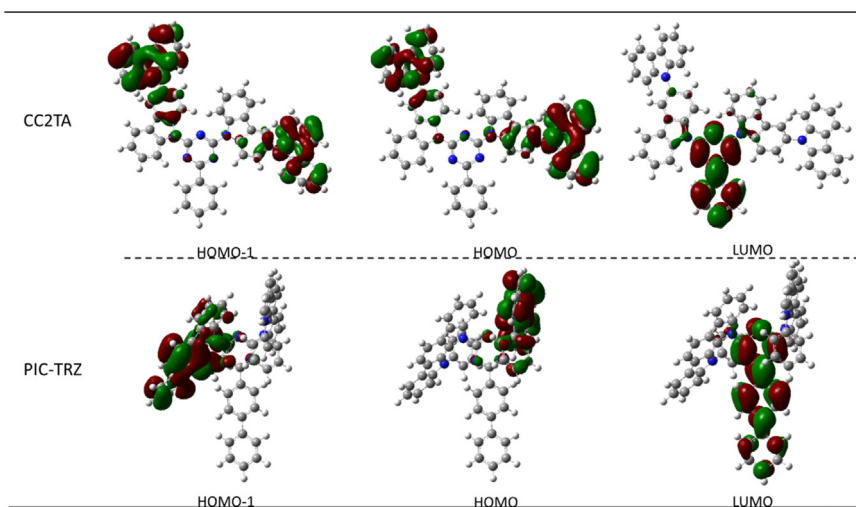


Fig. 3. Frontier molecular orbital distributions of CC2TA and PIC-TRZ.

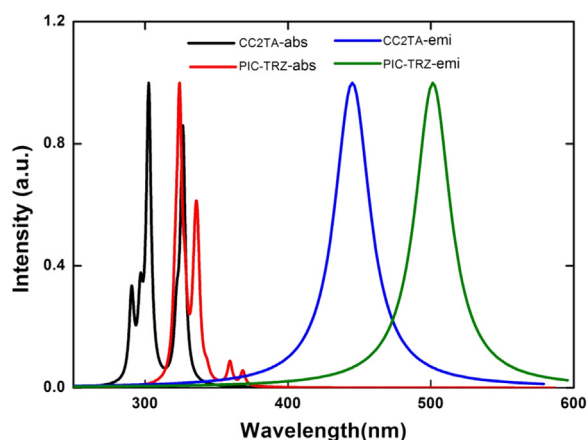


Fig. 4. UV-absorption and photoluminescence spectra of CC2TA and PIC-TRZ in toluene.

the following chapter.

4.3. Huang-Rhys factor and reorganization energy

The geometric modifications between S_0 and S_1 (T_1) play an important role in the photophysical properties because they can largely affect the non-radiative decay rate. Table 2 and Table 3 show the torsion angles which are marked out in Fig. 1. Through comparing the data, we know the angle of a1 and a3 change a small value ($0^\circ \sim 3^\circ$) when CC2TA transfers from S_0 to S_1 and then transfers to T_1 state. While a2, a4 and a5 show a large variation about 18° , and this indicates that the non-radiative decay process from S_1 to S_0 as well as T_1 to S_0 is mainly related to the rotation of phenyl and carbazole units. Moreover, the ISC and RISC processes are caused by the change of a2 from 35° in S_1 to 29° in T_1 . For PIC-TRZ, the main difference between S_0 , S_1 and T_1 is b6 which shows a significant rotation of phenyl (about 30°) at the end of acceptor unit. Moreover, as we know, the non-radiative decay rate

Table 2

Interesting angles (marked out in Fig. 1) are listed for CC2TA.

CC2TA	a1	a2	a3	a4	a5
S_0	19	21	122	121	12
S_1	20	35	119	138	3
T_1	21	29	119	139	4

Table 3

Interesting angles (marked out in Fig. 1) are listed for PIC-TRZ.

PIC-TRZ	b1	b2	b3	b4	b5	b6
S_0	138	58	117	45	4	37
S_1	135	60	119	45	0	30
T_1	138	60	117	45	2	0

constants of $S_1 \rightarrow S_0$, $T_1 \rightarrow S_0$ as well as $T_1 \leftrightarrow S_1$ are proportional the molecular deformation between S_0 and S_1 , S_0 and T_1 as well as T_1 and S_1 . In order to provide visible comparison, changes between S_0 , S_1 and T_1 are shown Fig. 5 for studied molecules. The root of the mean of squared displacement (RMSD) with the expression $\text{RMSD} = \sqrt{\frac{1}{N} \sum_i^{\text{natom}} [(x_i - x_i')^2 + (y_i - y_i')^2 + (z_i - z_i')^2]}$, is adopted to quantitatively characterize the geometric changes, a larger RMSD value means a bigger geometry change and the value of RMSD between two states is calculated by Multiwfn. For CC2TA and PIC-TRZ, the RMSD values are corresponding well with the geometry changes. Moreover, the RMSD value between S_0 and S_1 is 0.619 \AA for CC2TA, and it changes to 0.359 \AA for PIC-TRZ, this indicates that the PIC-TRZ molecule possesses a smaller non-radiative consumption of excited state. Similar condition can be seen between T_1 and S_0 with RMSD of 0.451 \AA for CC2TA and 0.321 \AA for PIC-TRZ, thus, a larger utilization of triplet excitons for PIC-TRZ can be expected.

In addition, the Huang-Rhys factors are calculated to demonstrate the molecular deformation for CC2TA and PIC-TRZ, because Huang-Rhys factor is a useful index for the extent of geometry relaxation between two electronic states, the HR factors are first calculated according to the equation $\text{HR}_k = \frac{\omega_k D_k^2}{2\hbar}$. Here, ω_k represents the vibration frequency and D_k is the normal coordinate displacement of mode k . Corresponding results are shown in Fig. S1 and Fig. S2, and HR factors are collected in Table 4. One point should be clarified, the value of RMSD represents the total geometry change between two states, here, we calculate the first three large HR factors ($S_{\text{max}1}$, $S_{\text{max}2}$, $S_{\text{max}3}$) and their total values (S_{all}). For CC2TA, we know the S_{all} is in the order of 35.2 (S_0 - S_1) $>$ 19.5 (S_0 - T_1) $>$ 3.3 (S_1 - T_1), that is corresponding well with the data of RMSD which is in the order of 0.619 \AA (S_0 - S_1) $>$ 0.451 \AA (S_0 - T_1) $>$ 0.209 \AA (S_1 - T_1). As for PIC-TRZ, the S_{all} is in the order of 22 (S_1 - T_1) $>$ 20.6 (S_0 - S_1) $>$ 18.6 (S_0 - T_1) with the order of RMSD 0.426 \AA (S_1 - T_1) $>$ 0.359 \AA (S_0 - S_1) $>$ 0.321 \AA (S_0 - T_1). Moreover, large HR factor means large non-radiative decay rate. Moreover, from Fig. S1 and Fig. S2, we know that large HR factors ($\text{HR} > 2$) are all appeared in low frequency regions ($< 500 \text{ cm}^{-1}$), and these vibrations are related to the rotation of outermost donor units. Furthermore, we

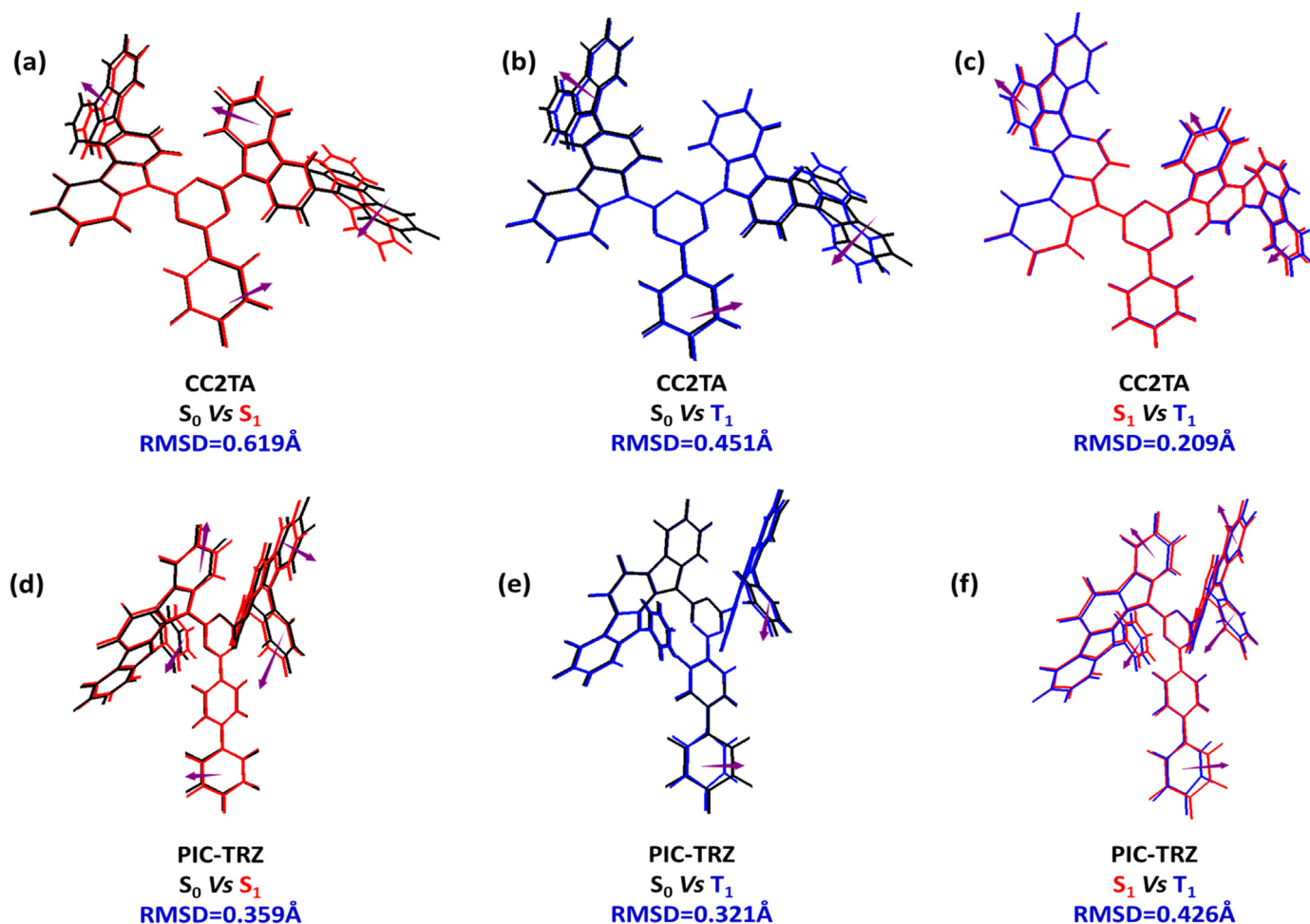


Fig. 5. Geometry comparisons between S₀ (black), S₁ (red) and T₁ (blue) of studied molecules. (For interpretation of the references to color in this figure legend, the reader is referred to the web version of this article).

Table 4

The first three large Huang-Rhys factor and their total values are list for CC2TA and PIC-TRZ respectively.

	CC2TA			PIC-TRZ		
	S ₀ -S ₁	S ₀ -T ₁	T ₁ -S ₁	S ₀ -S ₁	S ₀ -T ₁	T ₁ -S ₁
S _{max1}	17.4	13.1	2.2	10.1	8.6	7.8
S _{max2}	11.6	4.8	0.6	6.4	6.8	7.4
S _{max3}	6.2	1.6	0.5	4.1	3.2	6.8
S _{all}	35.2	19.5	3.3	20.6	18.6	22

investigate the reorganization energy versus the normal mode frequencies and corresponding results are shown in Fig. 6. Comparing all data, we can see that, the reorganization energy between S₁ and T₁ for CC2TA is small (Fig. 6c), this indicates that the geometry configuration of S₁ is similar to that of T₁, and this brings small HR factor (Fig. S1c). Furthermore, in order to better illustrate the relationship between molecular geometry and non-radiative energy dissipation, the reorganization energies are all projected onto the internal coordinate for CC2TA and PIC-TRZ. Contributions from bond length, bond angle and dihedral angle are collected in Table 5. Results show that the contribution from bond length takes the major part in composition of reorganization energy, for example, 71.7% for CC2TA between S₀ and S₁, and 61.6% for PIC-TRZ between S₁ and T₁. Moreover, a small reorganization energy for CC2TA between S₁ and T₁ can be found, this is corresponding well with the analysis of HR factor and RMSD. Such a large reorganization energy difference between S₁ and T₁ for CC2TA

and PIC-TRZ may result different up-conversion process and further affect the TADF properties.

4.4. Radiative and non-radiative decay rates

According to the equation $\lambda \propto \frac{H_{SO}}{\Delta E_{ST}}$ where λ is the first-order mixed coefficient between S₁ and T₁, and H_{SO} represents the spin-orbit coupling parameter, the ISC and RISC processes not only relate to the S₁-T₁ gap but also depend on the SOC constant. In this point, the heavy atoms are not required for TADF molecule to achieve efficient spin conversion when a molecule possesses a small ΔE_{ST} and H_{SO} is not vanishingly small. As discussed in Computation details, we calculate all rate parameters for the electroluminescence as shown in Fig. S3a, all data are collected in Table 6. Results show that, the calculated fluorescence rate for CC2TA is $1.91 \times 10^7 \text{ s}^{-1}$ which is larger than that for PIC-TRZ with fluorescence rate of $2.71 \times 10^6 \text{ s}^{-1}$, this may be caused by the enlarged symmetry distribution of HOMO for CC2TA, and this brings increased oscillator strength (0.0566) and further affects the luminescence property. As for the non-radiative decay rate of K_{nr}^S and K_{nr}^T , they are larger for CC2TA than these for PIC-TRZ. Moreover, the non-radiative rate K_{nr}^S exceeds reasonable limits compared with radiative decay rate K_r^S , this can result in non-emitting phenomenon which is contrary to the experimental results. The main reason is that, the non-radiative decay is sensitive to surroundings, our simulation is based on single molecular model and the intermolecular interaction is not considered. So when made into OLEDs, the molecular vibrations and structure changes as well as non-radiative process may be greatly reduced as illustrated in

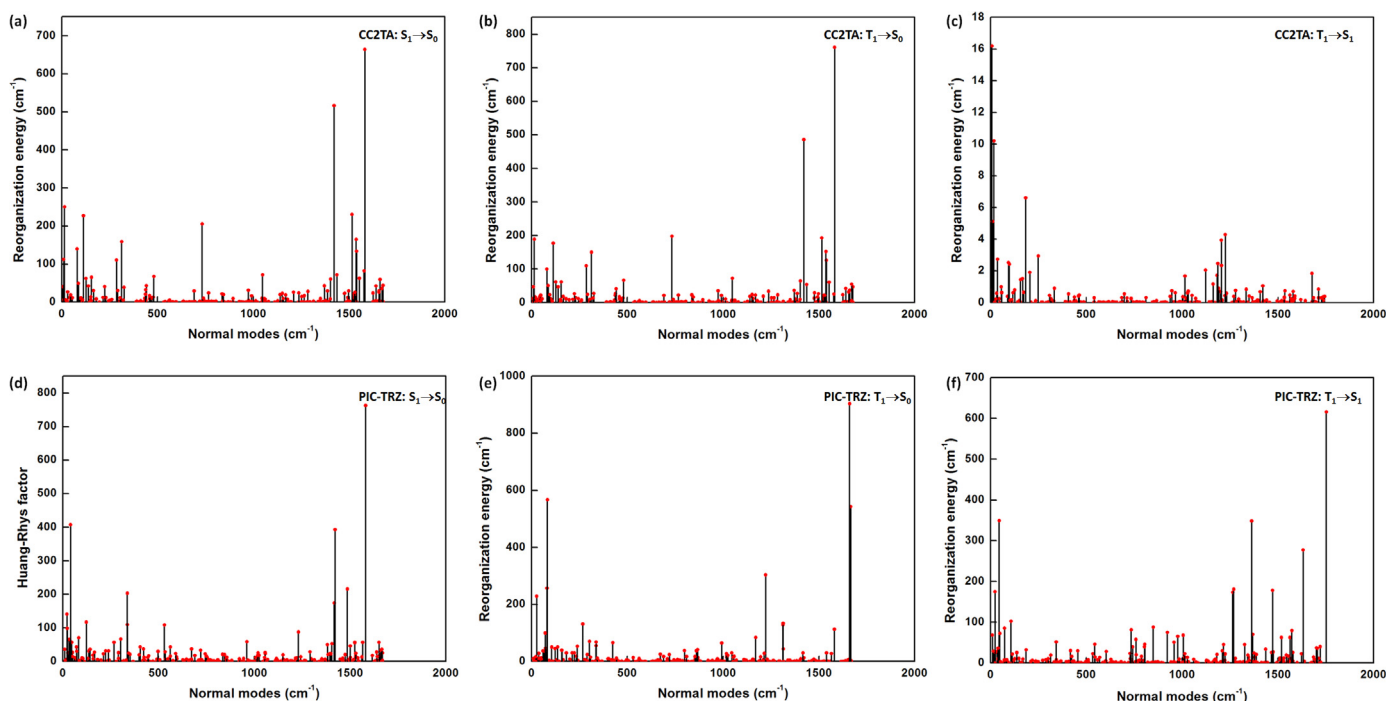


Fig. 6. Reorganization energy versus the normal modes wavenumber of CC2TA and PIC-TRZ.

Table 5

Reorganization energies (meV) from the bond length, bond angle, and dihedral angle for CC2TA and PIC-TRZ are listed respectively.

	CC2TA			PIC-TRZ		
	S ₀ -S ₁	S ₀ -T ₁	T ₁ -S ₁	S ₀ -S ₁	S ₀ -T ₁	T ₁ -S ₁
Bond length	442.7	433.6	5.5	422.9	490.5	398.1
Bond angle	112.3	115.2	0.3	158.5	7.1	114.6
Dihedral angle	82.4	55.6	8.0	105.0	178.6	134.0
All	617.4	604.4	13.8	686.4	676.2	646.7

previous work [23–25]. The accurate simulation of non-radiative process in organic film or organic crystal is being actively pursued.

As for the ISC and RISC processes, the calculated ISC rate is $4.07 \times 10^5 \text{ s}^{-1}$ and $4.89 \times 10^4 \text{ s}^{-1}$ for CC2TA and PIC-TRZ respectively, and the calculated RISC rate is $3.86 \times 10^5 \text{ s}^{-1}$ and $5.07 \times 10^2 \text{ s}^{-1}$ for CC2TA and PIC-TRZ respectively. Such efficient ISC and RISC processes are greatly related to the small S₁-T₁ gap (0.21 eV and 0.20 eV). Furthermore, as Jamie Gibson and Thomas J. Penfold point out, the vibronic coupling effect between the lowest local excitation triplet (³LE) and lowest charge transfer triplet (³CT) can facilitate the RISC for TADF [26–28], this illustrates the importance of intermediate energy level between S₁ and T₁. In order to illustrate this effect, we analyze the vertical excitation energy landscape of singlet and triplet states based on the optimized ground state, corresponding data are shown in Fig. S3b and Fig. S3c. When singlet and triplet excitons injected, they are converted to lowest excitons from the highly excited states through a rapid internal conversion process, mainly distributed in S₁ and T₁ state while the T₂ state will have some populations too for

CC2TA, because T₁ and T₂ are degenerate levels. The ISC process can take place not only from S₁ to T₁ directly, but also from S₁ to T₁₁ then to T₁. Meanwhile, for the RISC, it is also a multi-step process through additional energy level between S₁ and T₁, the ISC and RISC are multi-step processes. Here, the energy level is determined by the vertical excitation energy and this may be affected by different functionals, and the reasonable way is to calculate the adiabatic energy level for all excited states, this is a time-consuming process, and here we only provide a simple exposition for ISC and RISC processes.

5. Conclusion

In this work, two special TADF molecules of CC2TA and PIC-TRZ are theoretically investigated to illustrate their photophysical properties and internal transfer mechanism of singlet and triplet excitons. Based on the optimal Hartree-Fock method, we calculated the adiabatic energy gap, absorption and emission spectra. All data are corresponding well with the experimental results, this verifies the reliability of our adopted method for two molecules. Moreover, the index of RMSD, HR factor and reorganization energy are used to analyze the non-radiative consumption of excited energy. Results show that the non-radiative decay rates K_{nr}^s , K_{nr}^t , K_{ISC} and K_{RISC} for PIC-TRZ are all smaller than these for CC2TA, this is largely caused by the smaller geometry changes between S₀, S₁ and T₁ of PIC-TRZ. Furthermore, the ISC and RISC processes are multi-step processes with the incorporation of intermediate energy level between S₁ and T₁. We theoretically provide illustrations for photophysical properties of two special TADF molecules, which is beneficial to design more efficient TADF molecules.

Table 6

The calculated oscillator strengths (f) and radiative (K_r^s) and non-radiative decay rate (K_{nr}^s) from S₁ to S₀, K_{ISC} and K_{RISC} represents the intersystem crossing and reverse intersystem crossing rate between S₁ and T₁. K_r^t and K_{nr}^t is the radiative and non-radiative decay rate from T₁ to S₀ respectively. (unit s⁻¹).

	f	K_r^s	K_{nr}^s	K_{ISC}	K_{RISC}	K_r^t	K_{nr}^t
CC2TA	0.0566	1.91×10^7	3.47×10^{14}	4.07×10^5	3.86×10^5	4.64×10^{-2}	1.18×10^7
PIC-TRZ	0.0102	2.71×10^6	1.14×10^{11}	4.89×10^4	5.07×10^2	4.14×10^{-2}	1.18×10^4

Acknowledgements

This work is supported by the National Natural Science Foundation of China (Grant No.11704209), Shandong Province Program on Key Research Projects (Grant No. 2015GGX101017) and the Excellent Young Scholars Research Fund of Shandong Normal University. Great thanks to Professor Chuankui Wang and Lili Lin for their helpful suggestions in our calculation.

Appendix A. Supporting information

Supplementary data associated with this article can be found in the online version at <https://doi.org/10.1016/j.jlumin.2018.07.012>.

References

- [1] H. Uoyama, K. Goushi, K. Shizu, H. Nomura, C. Adachi, *Nature* 492 (2012) 234.
- [2] L.-S. Cui, S.-B. Ruan, F. Bencheikh, R. Nagata, L. Zhang, K. Inada, H. Nakanotani, L.-S. Liao, C. Adachi, *Nat. Commun.* 8 (2017) 2250.
- [3] J. Zhang, W. Chen, R. Chen, X.-K. Liu, Y. Xiong, S.V. Kershaw, A.L. Rogach, C. Adachi, X. Zhang, C.-S. Lee, *Chem. Commun.* 52 (2016) 11744.
- [4] J. Huang, H. Nie, J. Zeng, Z. Zhuang, S. Gan, Y. Cai, J. Guo, S.J. Su, Z. Zhao, B.Z. Tang, *Angew. Chem.* 129 (2017) 13151.
- [5] M. Liu, R. Komatsu, X. Cai, H. Sasabe, T. Kamata, K. Nakao, K. Liu, S.J. Su, J. Kido, *Adv. Opt. Mater.* 5 (2017) 19.
- [6] Y. Zhang, D. Zhang, M. Cai, Y. Li, Y. Qiu, L. Duan, *Nanotechnology* 27 (2016) 094001.
- [7] K. Kawasumi, T. Wu, T. Zhu, H.S. Chae, T. Van Voorhis, M.A. Baldo, T.M. Swager, *J. Am. Chem. Soc.* 137 (2015) 11908.
- [8] S. Youn Lee, T. Yasuda, H. Nomura, C. Adachi, *Appl. Phys. Lett.* 101 (2012) 093306.
- [9] A. Endo, K. Sato, K. Yoshimura, T. Kai, A. Kawada, H. Miyazaki, C. Adachi, *Appl. Phys. Lett.* 98 (2011) 42.
- [10] Y. Tao, K. Yuan, T. Chen, P. Xu, H. Li, R. Chen, C. Zheng, L. Zhang, W. Huang, *Adv. Mater.* 26 (2014) 7931.
- [11] Q. Peng, Q. Shi, Y. Niu, Y. Yi, S. Sun, W. Li, Z. Shuai, *J. Mater. Chem. C* 4 (2016) 6829.
- [12] Y. Niu, Q. Peng, C. Deng, X. Gao, Z. Shuai, *J. Phys. Chem. A* 114 (2010) 7817.
- [13] Z. Shuai, Q. Peng, *Phys. Rep.* 537 (2014) 123.
- [14] L. Lin, J. Fan, C.-K. Wang, *Org. Electron.* 51 (2017) 349.
- [15] J. Fan, L. Lin, C.-K. Wang, *J. Mater. Chem. C* 5 (2017) 8390.
- [16] S. Huang, Q. Zhang, Y. Shiota, T. Nakagawa, K. Kuwabara, K. Yoshizawa, C. Adachi, *J. Chem. Theory Comput.* 9 (2013) 3872.
- [17] T. Lu, F. Chen, *J. Comput. Chem.* 33 (2012) 580.
- [18] (a) M.J. Frisch, G.W. Trucks, H.B. Schlegel, G.E. Scuseria, M.A. Robb, J.R. Cheeseman, G. Scalmani, V. Barone, B. Mennucci, G.A. Petersson, Gaussian 09, Revision A.02, Gaussian, Inc, 2009.
(b) G.W.T.M.J. Frisch, H.B. Schlegel, G.E. Scuseria, M.A. Robb, J.R. Cheeseman, G. Scalmani, V. Barone, B. Mennucci, G.A. Petersson, H. Nakatsuji, M. Caricato, X. Li, H.P. Hratchian, A.F. Izmaylov, J. Bloino, G. Zheng, J.L. Sonnenberg, M. Hada, M. Ehara, K. Toyota, R. Fukuda, J. Hasegawa, M. Ishida, T. Nakajima, Y. Honda, O. Kitao, H. Nakai, T. Vreven, J.A. Montgomery, Jr., J.E. Peralta, F. Ogliaro, M. Bearpark, J.J. Heyd, E. Brothers, K.N. Kudin, V.N. Staroverov, R. Kobayashi, J. Normand, K. Raghavachari, A. Rendell, J.C. Burant, S. S. Iyengar, J. Tomasi, M. Cossi, N. Rega, J.M. Millam, M. Klene, J.E. Knox, J.B. Cross, V. Bakken, C. Adamo, J. Jaramillo, R. Gomperts, R.E. Stratmann, O. Yazyev, A.J. Austin, R. Cammi, C. Pomelli, J.W. Ochterski, R.L. Martin, K. Morokuma, V.G. Zakrzewski, G.A. Voth, P. Salvador, J.J. Dannenberg, S. Dapprich, A.D. Daniels, O. Farkas, J.B. Foresman, J.V. Ortiz, J. Cioslowski, D.J. Fox, Gaussian09 Revision A.01, Gaussian Inc., Wallingford CT, 2009.
- [19] DALTON: A molecular electronic structure program <<http://daltonprogram.org/>>.
- [20] T. Zhang, H. Ma, Y. Niu, W. Li, D. Wang, Q. Peng, Z. Shuai, W. Liang, *J. Phys. Chem. C* 119 (2015) 5040.
- [21] Z. He, W. Zhao, J.W. Lam, Q. Peng, H. Ma, G. Liang, Z. Shuai, B.Z. Tang, *Nat. Commun.* 8 (2017) 416.
- [22] Q. Peng, D. Fan, R.-H. Duan, Y. Yi, Y. Niu, D. Wang, Z. Shuai, *J. Phys. Chem. C* (2017).
- [23] J. Fan, L. Cai, L. Lin, C.-K. Wang, *Phys. Chem. Chem. Phys.* 19 (2017) 29872.
- [24] I.H. Lee, W. Song, J.Y. Lee, *Org. Electron.* 29 (2016) 22.
- [25] B. Liu, H. Nie, X. Zhou, S. Hu, D. Luo, D. Gao, J. Zou, M. Xu, L. Wang, Z. Zhao, *Adv. Funct. Mater.* 26 (2016) 776.
- [26] J. Gibson, T. Penfold, *Phys. Chem. Chem. Phys.* 19 (2017) 8428.
- [27] J. Gibson, A.P. Monkman, T.J. Penfold, *ChemPhysChem* 17 (2016) 2956.
- [28] M.K. Etherington, J. Gibson, H.F. Higginbotham, T.J. Penfold, A.P. Monkman, *Nat. Commun.* 7 (2016) 13680.